

Contents lists available at [ScienceDirect](http://www.sciencedirect.com)

# Journal of Sound and Vibration

journal homepage: [www.elsevier.com/locate/jsvi](http://www.elsevier.com/locate/jsvi)

## Free vibration analysis of an eccentric hollow cylinder using exact 3D elasticity theory

Seyyed M. Hasheminejad\*, Yaser Mirzaei

Acoustics Research Laboratory, Department of Mechanical Engineering, Iran University of Science and Technology, Narmak, Tehran 16844, Iran

### ARTICLE INFO

#### Article history:

Received 12 February 2009

Received in revised form

9 May 2009

Accepted 13 May 2009

Handling Editor: C.L. Morfey

Available online 6 June 2009

### ABSTRACT

The translational addition theorem for cylindrical wave functions in conjunction with the appropriate orthogonal series expansions and the pertinent boundary conditions are employed to develop an exact 3D elasticity solution for free vibrations of a simply (shear diaphragm) supported elastic circular cylinder of finite length with an eccentrically located inner circular cavity. The frequency spectrum plots of the first several eigenfrequencies are presented in a wide range of dimensionless eccentricities for selected length-to-radius and inner–outer radius ratios. Also, a detailed study on the 2D free vibration characteristics of an infinite eccentric cylinder is included. The numerical results describe the imperative influence of cavity eccentricity, mode type, and radii and length ratios on the vibrational characteristics of the hollow cylinder. It is observed that the introduction of bore eccentricity causes not only an increase in the number of resonant frequencies through the splitting of degenerate modes of the unperturbed problem, but also changes the appearance order of natural vibration modes. The accuracy of solutions is checked through appropriate convergence studies, and the validity of results is established with the aid of a commercial finite element package as well as by comparison with the data in the existing literature.

© 2009 Elsevier Ltd. All rights reserved.

### 1. Introduction

Many of studies on the dynamic behavior of cylindrical shells in the literature are based on classical or thin-shell theories. These theories utilize the simplifying assumptions of Kirchhoff–Love's hypothesis (i.e., ignorance of the transverse stress and strain components), making them highly inadequate for the analysis of even slightly thick shells. In recent years, the refinement of thin-shell theories has resulted in a number of the so-called higher order shell theories [1]. The higher order shell theories are better than the thin-shell theories for the analysis of slightly thick shells but are still inadequate for the analysis of moderately thick shells. This makes the use of 3D theory of elasticity for dynamic analysis of these structures inevitable. Computer performance being the only limiting factor, the 3D theory of elasticity can particularly be used to find accurate values for the natural vibration frequencies of solid or thick hollow elastic cylinders. Such analysis provides, not only reliable solutions, but also brings out the physical characteristics of the problem [2].

The first known 3D elasticity solution to the free (axisymmetric) vibrations of an infinitely long ideal elastic circular cylinder with stress-free lateral surface condition was attributed to Pochhammer in 1876 [3]. The 3D vibration problem of a finite cylinder is much more complicated. Several researchers have carried out such analysis based on the linear equations of elasticity in order to find accurate natural frequencies for the vibrations of solid or hollow thick isotropic cylinders of finite length. Among them, Hutchinson and El-Azhari [4] developed a highly accurate semi-analytical method using Bessel

\* Corresponding author. Tel.: +98 912 7371354; fax: +98 21 77240488.

E-mail address: [hashemi@iust.ac.ir](mailto:hashemi@iust.ac.ir) (S.M. Hasheminejad).

series solution method to solve for the symmetric and unsymmetric vibrations of finite length traction-free hollow cylinders. Loy and Lam [5] presented an approximate analysis using a layerwise approach to study the vibration of thick simply supported and clamped circular cylindrical shells. More recently, Mofakhami et al. [6] employed the separation of variables technique to develop a general semi-analytical solution for the free vibrations of hollow finite cylinders with “free-end” and “fixed-end” boundary conditions.

Axisymmetric structures are commonly used in engineering applications, as computer memory disks, turbine-bladed disks, ring gyroscopes, machine elements, structural components, gun tubes, pipes, pressure vessels, and so on. It is well known that when structural irregularities (e.g., dimensional variations, manufacturing tolerances, and material nonuniformities) are present, the symmetry of the structure is destroyed, the pairs of degenerate eigenfrequencies which are coincident in the perfectly symmetric case split into two different values, and the mechanical performance may severely be diminished [7]. Numerous papers in the open literature are devoted to the influence of various types of imperfections or geometric asymmetries on the vibration characteristics of (nominally) axisymmetric structures. In particular, great efforts have been spent for quantitative evaluation of the frequency split and modal shape distortion in imperfect rings and annular-like (eccentric) plates or disks. For example, Khurasia and Rewtant [8] used finite-element method to examine the effect of presence of an eccentric hole on free vibrations of a thin circular plate. Laura et al. [9] employed Rayleigh–Ritz and finite element methods to determine the effect of circumferential variations in wall thickness on eigenfrequencies and axisymmetric modes of a nonuniform ring. Hwang et al. [10] used the Novozhilov’s thin-shell theory and Rayleigh–Ritz analysis to study the effects of general in-plane cross sectional profile variations of a thin ring on its free vibration characteristics. More recently, Cheng et al. [7] employed a commercial finite element analysis code along with experimental modal analysis to study the effects of boundary condition, cutout eccentricity and size and on vibration modes of an annular-like plate. Also, Zhong and Yu [11] adopted a weak-form quadrature element method to study the flexural free vibrations of a moderately thick (Mindlin) eccentric annular plate with typical combinations of boundary conditions.

In contrast with the nonuniform ring or eccentric plate (disk) problem, relatively few researchers have addressed the effects of circumferential wall thickness variation on the vibrational behavior of cylindrical shells (eccentric cylinders). The most important works directly relevant to the present study shall be briefly reviewed here. Golovchan [12] developed an exact elasticity solution for the steady forced vibrations of an elastic body that occupies a finite multiply connected 2D region with circular boundaries. Quantitative results were presented only for low-frequency vibrations of an infinitely long eccentric cylinder subject to an external or internal pressure load. Tonin and Bins [13] used Love’s thin-shell theory in conjunction with the Rayleigh–Ritz method to approximate the natural frequencies of a finite length distorted circular cylindrical shell with circumferential wall thickness variations and shear diaphragm end conditions. Suzuki and Leissa [14,15] employed thin and thick shell theories in conjunction with power series expansion method to formulate an exact solution procedure for determining the free vibration frequencies and mode shapes of circular and noncircular (elliptical) cylindrical shells of circumferentially varying thickness having shear diaphragm end conditions. Kumar and Singh [16] utilized Bezier functions in Ritz method along with Kirchhoff–Love classical thin-shell theory to study the free vibrations of noncircular (elliptic and oval) cylindrical shells having a circumferentially varying thickness, with various boundary conditions. They focused on overcoming the mathematical difficulties associated with mode coupling between the symmetric and antisymmetric vibration modes caused by variable shell wall curvature and thickness. More recently, Toorani and Lakis [17] used a combination of hybrid finite element method and the thick shell theory to present a semi-analytical free vibration analysis of laminated, anisotropic, and circumferentially uniform or nonuniform cylindrical shells with arbitrary boundary conditions.

The above review indicates that while there exists a notable (reasonable) body of literature on free vibrations of eccentric rings and plates (cylindrical shells with circumferentially varying thickness), rigorous analytic or numerical solutions for a finite length cylinder with an eccentric inner circular cavity seems to be nonexistent (see Fig. 1). Accordingly, the main purpose of the current work is to employ the translational addition theorem for cylindrical wave functions along with the appropriate orthogonal series expansions and the pertinent boundary conditions to develop an exact elasticity solution for the proposed problem. The eccentric cylindrical components are extensively used as the basic structural elements in many engineering applications such as machining parts, electric devices, machinery, gun tubes, pipes, pressure vessels, etc. [18,19]. Thus, a comprehensive dynamic characterization of such structures will provide a real basis for the design engineer in assessing the suitability of introducing cavities in these elements at each situation. It can particularly provide guidance on vibration measurement and control, structural parameter identification, occurrence of vibration localization and damage detection in such structures [7,20]. The proposed model is also of fundamental interest due to its inherent value as a canonical problem in structural dynamics. Furthermore, the presented exact solution can serve as the benchmark for comparison to other solutions obtained by the generally restrictive numerical or asymptotic approaches.

## 2. Formulation

### 2.1. Basic field equations

The elastic material under consideration is assumed to be linear, macroscopically homogeneous, and isotropic for which the constitutive equation may be written as

$$\sigma_{ij} = \lambda \delta_{ij} \varepsilon + 2\mu \varepsilon_{ij}, \quad (1)$$

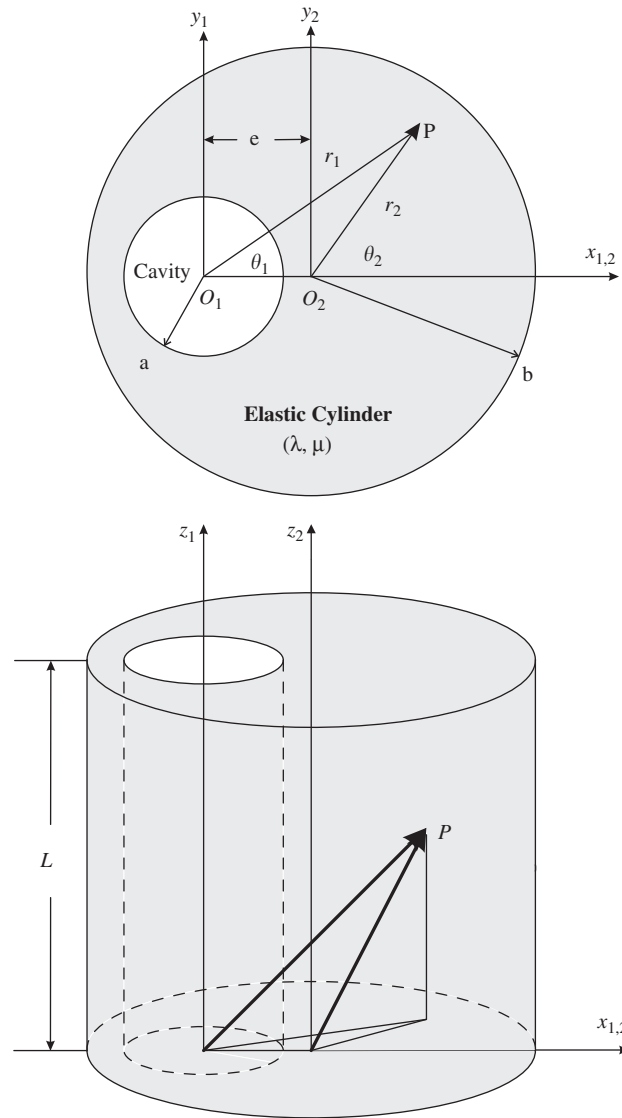


Fig. 1. Problem geometry.

where  $\delta_{ij}$  is Kronecker delta symbol and  $(\lambda, \mu)$  are Lamé constants. The problem can be analyzed by means of the standard methods of elastodynamics. In the absence of body forces, the displacement field is governed by the classical Navier's equation [21]

$$\rho \frac{\partial^2 \mathbf{u}}{\partial t^2} = \mu \nabla^2 \mathbf{u} + (\lambda + \mu) \nabla (\nabla \cdot \mathbf{u}), \tag{2}$$

subject to the appropriate boundary conditions. Here,  $\rho$  is the solid material density, and  $\mathbf{u} = (u_r, u_\theta, u_z)$  is the vector displacement that can advantageously be expressed as sum of the gradient of a scalar potential and the curl of a vector potential

$$\mathbf{u} = \nabla \varphi + \nabla \times \boldsymbol{\psi}, \tag{3}$$

with the condition  $\nabla \cdot \boldsymbol{\psi} = 0$ . The above decomposition enables us to separate the dynamic equation of motion (2) into the classical wave equations

$$\begin{aligned} c_p^2 \nabla^2 \varphi &= \ddot{\varphi}, \\ c_s^2 \nabla^2 \boldsymbol{\psi} &= \ddot{\boldsymbol{\psi}}, \end{aligned} \tag{4}$$

where  $c_p^2 = (\lambda + 2\mu)/\rho$  and  $c_s^2 = \mu/\rho$  are the propagation velocities of dilatational and distortional waves in the elastic medium, respectively. On the account of the condition of zero divergence,  $\nabla \cdot \psi = 0$ , only two of the three components of  $\psi$  are independent. Accordingly, the above system (4) may be reduced to the following fully uncoupled scalar wave equations [21]

$$\begin{aligned}c_p^2 \nabla^2 \varphi &= \ddot{\varphi}, \\c_s^2 \nabla^2 \psi &= \ddot{\psi}, \\c_s^2 \nabla^2 \chi &= \ddot{\chi}.\end{aligned}\quad (5)$$

Furthermore, the relevant displacement components in cylindrical coordinates in terms of compressional and shear wave potentials may simply written as [21]

$$\begin{aligned}u_r &= \frac{\partial \varphi}{\partial r} + \frac{1}{r} \frac{\partial \psi}{\partial \theta} + \frac{\partial^2 \chi}{\partial r \partial z}, \\u_\theta &= \frac{1}{r} \frac{\partial \varphi}{\partial \theta} - \frac{\partial \psi}{\partial r} + \frac{1}{r} \frac{\partial^2 \chi}{\partial \theta \partial z}, \\u_z &= \frac{\partial \varphi}{\partial z} - \left[ \frac{1}{r} \frac{\partial}{\partial r} \left( r \frac{\partial \chi}{\partial r} \right) + \frac{1}{r^2} \frac{\partial^2 \chi}{\partial \theta^2} \right],\end{aligned}\quad (6)$$

and the relevant stress components are

$$\begin{aligned}\sigma_{rr} &= \lambda \nabla^2 \varphi + 2\mu \left[ \frac{\partial^2 \varphi}{\partial r^2} + \frac{\partial}{\partial r} \left( \frac{1}{r} \frac{\partial \psi}{\partial \theta} \right) + \frac{\partial^3 \chi}{\partial r^2 \partial z} \right], \\ \sigma_{zz} &= \lambda \nabla^2 \varphi + 2\mu \left[ \frac{\partial^2 \varphi}{\partial z^2} - \frac{\partial}{\partial z} (\nabla^2 \chi) + \frac{\partial^3 \chi}{\partial z^3} \right], \\ \sigma_{r\theta} &= \mu \left\{ 2 \frac{\partial}{\partial r} \left( \frac{1}{r} \frac{\partial \varphi}{\partial \theta} \right) + \left[ \frac{1}{r^2} \frac{\partial^2 \psi}{\partial \theta^2} - r \frac{\partial}{\partial r} \left( \frac{1}{r} \frac{\partial \psi}{\partial r} \right) \right] + 2 \frac{\partial}{\partial r} \left( \frac{1}{r} \frac{\partial^2 \chi}{\partial z \partial \theta} \right) \right\}, \\ \sigma_{rz} &= \mu \left\{ 2 \frac{\partial^2 \varphi}{\partial r \partial z} + \frac{1}{r} \frac{\partial^2 \psi}{\partial \theta \partial z} + \left[ 2 \frac{\partial^3 \chi}{\partial z^2 \partial r} - \frac{\partial}{\partial r} (\nabla^2 \chi) \right] \right\}.\end{aligned}\quad (7)$$

## 2.2. Field expansions and boundary conditions

The problem geometry is depicted in Fig. 1. Two cylindrical coordinates systems  $(r_1, \theta_1, z_1)$  and  $(r_2, \theta_2, z_2)$  are introduced to describe the elastic field within the eccentric cylinder. The cylinder axes are parallel, and  $z_1 = z_2 = z$ . Their origin-to-origin separation is  $e$  ( $e_{\max} = b - a$ ), and point  $P$  is an arbitrary field point within the eccentric cylinder, outside the cylindrical cavity. Assuming time-harmonic variations, the field expansions for the standing longitudinal and shear waves within the eccentric cylinder (i.e., the solutions to the wave Eqs. (5)) with respect to the  $(r_1, \theta_1, z)$  coordinate system may be written as [21]

$$\begin{aligned}\varphi(r_1, \theta_1, z, \omega) &= \sum_{m=-\infty}^{\infty} \sum_{n=-\infty}^{\infty} [a_{nm} J_n(\alpha r_1) + b_{nm} Y_n(\alpha r_1)] \sin(\gamma z) e^{in\theta_1}, \\ \psi(r_1, \theta_1, z, \omega) &= \sum_{m=-\infty}^{\infty} \sum_{n=-\infty}^{\infty} [c_{nm} J_n(\beta r_1) + d_{nm} Y_n(\beta r_1)] \cos(\gamma z) e^{in\theta_1}, \\ \chi(r_1, \theta_1, z, \omega) &= \sum_{m=-\infty}^{\infty} \sum_{n=-\infty}^{\infty} [e_{nm} J_n(\beta r_1) + f_{nm} Y_n(\beta r_1)] \cos(\gamma z) e^{in\theta_1},\end{aligned}\quad (8)$$

where  $i = \sqrt{-1}$ ,  $a_{nm}$  through  $f_{nm}$  are unknown modal coefficients,  $\alpha^2 = \omega^2/c_p^2 - \gamma^2$ ,  $\beta^2 = \omega^2/c_s^2 - \gamma^2$ ,  $J_n$  and  $Y_n$  are the cylindrical Bessel functions of the first and second kind, respectively, and  $(\alpha, \gamma, \beta)$  are separation constants. Direct

substitution of field expansions (8) into the field equations (6) and (7), leads to

$$\begin{aligned}
 u_r(r_1, \theta_1, z, \omega) &= \sum_{m=-\infty}^{\infty} \sum_{n=-\infty}^{\infty} (a_{nm}V_{1n}^{[1]} + b_{nm}V_{1n}^{[2]} + c_{nm}V_{2n}^{[1]} + d_{nm}V_{2n}^{[2]} + e_{nm}V_{3n}^{[1]} + f_{nm}V_{3n}^{[2]}) \sin(\gamma z)e^{in\theta_1}, \\
 u_{\theta}(r_1, \theta_1, z, \omega) &= \sum_{m=-\infty}^{\infty} \sum_{n=-\infty}^{\infty} (a_{nm}V_{4n}^{[1]} + b_{nm}V_{4n}^{[2]} + c_{nm}V_{5n}^{[1]} + d_{nm}V_{5n}^{[2]} + e_{nm}V_{6n}^{[1]} + f_{nm}V_{6n}^{[2]}) \sin(\gamma z)e^{in\theta_1}, \\
 u_z(r_1, \theta_1, z, \omega) &= \sum_{m=-\infty}^{\infty} \sum_{n=-\infty}^{\infty} (a_{nm}V_{7n}^{[1]} + b_{nm}V_{7n}^{[2]} + c_{nm}V_{8n}^{[1]} + d_{nm}V_{8n}^{[2]} + e_{nm}V_{9n}^{[1]} + f_{nm}V_{9n}^{[2]}) \cos(\gamma z)e^{in\theta_1} \tag{9}
 \end{aligned}$$

and

$$\begin{aligned}
 \sigma_{rr}(r_1, \theta_1, z, \omega) &= \sum_{m=-\infty}^{\infty} \sum_{n=-\infty}^{\infty} (a_{nm}S_{1n}^{[1]} + b_{nm}S_{1n}^{[2]} + c_{nm}S_{2n}^{[1]} + d_{nm}S_{2n}^{[2]} + e_{nm}S_{3n}^{[1]} + f_{nm}S_{3n}^{[2]}) \sin(\gamma z)e^{in\theta_1}, \\
 \sigma_{r\theta}(r_1, \theta_1, z, \omega) &= \sum_{m=-\infty}^{\infty} \sum_{n=-\infty}^{\infty} (a_{nm}S_{4n}^{[1]} + b_{nm}S_{4n}^{[2]} + c_{nm}S_{5n}^{[1]} + d_{nm}S_{5n}^{[2]} + e_{nm}S_{6n}^{[1]} + f_{nm}S_{6n}^{[2]}) \sin(\gamma z)e^{in\theta_1}, \\
 \sigma_{rz}(r_1, \theta_1, z, \omega) &= \sum_{m=-\infty}^{\infty} \sum_{n=-\infty}^{\infty} (a_{nm}S_{7n}^{[1]} + b_{nm}S_{7n}^{[2]} + c_{nm}S_{8n}^{[1]} + d_{nm}S_{8n}^{[2]} + e_{nm}S_{9n}^{[1]} + f_{nm}S_{9n}^{[2]}) \cos(\gamma z)e^{in\theta_1}, \\
 \sigma_{zz}(r_1, \theta_1, z, \omega) &= \sum_{m=-\infty}^{\infty} \sum_{n=-\infty}^{\infty} (a_{nm}S_{10n}^{[1]} + b_{nm}S_{10n}^{[2]} + c_{nm}S_{11n}^{[1]} + d_{nm}S_{11n}^{[2]} + e_{nm}S_{12n}^{[1]} + f_{nm}S_{12n}^{[2]}) \sin(\gamma z)e^{in\theta_1}, \tag{10}
 \end{aligned}$$

where the expressions for  $V_{in}^{[k]}(r_j, \gamma, \omega)$  ( $i = 1, 2, \dots, 9; j, k = 1, 2$ ) and  $S_{in}^{[k]}(r_j, \gamma, \omega)$  ( $i = 1, 2, \dots, 12; j, k = 1, 2$ ) are given in Appendix A.

The natural frequencies and the unknown Fourier coefficients may be determined by imposing the proper boundary conditions. Accordingly, assuming shear diaphragm end conditions [1], and traction-free inner/outer surfaces, one can write (see Fig. 1)

$$u_r(r_i; \theta_i; z = 0, L; \omega) = u_{\theta}(r_i; \theta_i; z = 0, L; \omega) = \sigma_{zz}(r_i; \theta_i; z = 0, L; \omega) = 0, \tag{11a}$$

$$\sigma_{rr}(r_1 = a; \theta_1; z; \omega) = \sigma_{r\theta}(r_1 = a; \theta_1; z; \omega) = \sigma_{rz}(r_1 = a; \theta_1; z; \omega) = 0, \tag{11b}$$

$$\sigma_{rr}(r_2 = b; \theta_2; z; \omega) = \sigma_{r\theta}(r_2 = b; \theta_2; z; \omega) = \sigma_{rz}(r_2 = b; \theta_2; z; \omega) = 0, \tag{11c}$$

where  $i = 1, 2$ . Using first two of (9) and last of (10) in satisfaction of the boundary conditions (11a) leads to the simple condition  $\gamma = \gamma_m = m\pi/L$  ( $m = \dots, -2, -1, 0, 1, 2, \dots$ ). Also, using (10), enforcement of the inner surface boundary condition (11b) leads to the following equations:

$$\begin{aligned}
 a_{nm}S_{1nm}^{[1]}(a, \omega) + b_{nm}S_{1nm}^{[2]}(a, \omega) + c_{nm}S_{2nm}^{[1]}(a, \omega) + d_{nm}S_{2nm}^{[2]}(a, \omega) + e_{nm}S_{3nm}^{[1]}(a, \omega) + f_{nm}S_{3nm}^{[2]}(a, \omega) &= 0, \\
 a_{nm}S_{4nm}^{[1]}(a, \omega) + b_{nm}S_{4nm}^{[2]}(a, \omega) + c_{nm}S_{5nm}^{[1]}(a, \omega) + d_{nm}S_{5nm}^{[2]}(a, \omega) + e_{nm}S_{6nm}^{[1]}(a, \omega) + f_{nm}S_{6nm}^{[2]}(a, \omega) &= 0, \\
 a_{nm}S_{7nm}^{[1]}(a, \omega) + b_{nm}S_{7nm}^{[2]}(a, \omega) + c_{nm}S_{8nm}^{[1]}(a, \omega) + d_{nm}S_{8nm}^{[2]}(a, \omega) + e_{nm}S_{9nm}^{[1]}(a, \omega) + f_{nm}S_{9nm}^{[2]}(a, \omega) &= 0, \tag{12}
 \end{aligned}$$

where  $n, m = \dots, -2, -1, 0, 1, 2, \dots$ , and  $S_{inn}^{[k]}(r_j, \omega) = S_{in}^{[k]}(r_j, \gamma_m, \omega)$ ; ( $i = 1, 2, \dots, 12; j, k = 1, 2$ ). Satisfaction of the outer boundary condition (11c) is far more complicated, and will be achieved next by application of the translational addition theorem for cylindrical wave functions.

### 2.3. Translational addition theorem

Analytical solutions of interior or exterior boundary value problems in various fields such as potential theory, elastodynamics, acoustics and electromagnetism are strictly dependent on the shape of boundaries. In particular, when multiple interfaces are present in a wave field, there is an interaction between them due to cross scattering. Many problems involve wave fields of one characteristic shape (coordinate system) that interact with a boundary of some other shape (coordinate system). So it is difficult to satisfy the boundary conditions on that surface. There exists, however, a particular class of mathematical relationships called translational addition theorems that circumvents this difficulty in many cases by allowing one to study various wave fields with respect to a common origin. To fulfill orthogonality in the current problem, we shall express the cylindrical wave functions of the first coordinate system  $(r_1, \theta_1, z)$  in terms of cylindrical wave functions of the second coordinate system  $(r_2, \theta_2, z)$  by application of the classical form of translational addition theorem

for cylindrical Bessel functions [22]:

$$\begin{Bmatrix} J_n(\kappa r_1) \\ Y_n(\kappa r_1) \end{Bmatrix} e^{in\theta_1} = \sum_{k=-\infty}^{\infty} J_{n-k}(\kappa e) \begin{Bmatrix} J_n(\kappa r_2) \\ Y_n(\kappa r_2) \end{Bmatrix} e^{ik\theta_2}, \quad (13)$$

where  $e < r_2$  ( $0 \leq r_2 \leq b$ ), and noting  $e_{\max} = b - a$ , when later imposing the relevant boundary conditions at  $r_2 = b$ , the condition  $e < r_2 = b$  will be clearly satisfied. The above expansion may advantageously be utilized in (8) in order to express the field potentials with respect to the second coordinate system, i.e.,

$$\begin{aligned} \varphi(r_2, \theta_2, z, \omega) &= \sum_{m=-\infty}^{\infty} \sum_{n=-\infty}^{\infty} [A_{mn} J_n(\alpha r_2) + B_{mn} Y_n(\alpha r_2)] e^{in\theta_2} \sin(\gamma_m z), \\ \psi(r_2, \theta_2, z, \omega) &= \sum_{m=-\infty}^{\infty} \sum_{n=-\infty}^{\infty} [C_{mn} J_n(\beta r_2) + D_{mn} Y_n(\beta r_2)] e^{in\theta_2} \cos(\gamma_m z), \\ \chi(r_2, \theta_2, z, \omega) &= \sum_{m=-\infty}^{\infty} \sum_{n=-\infty}^{\infty} [E_{mn} J_n(\beta r_2) + F_{mn} Y_n(\beta r_2)] e^{in\theta_2} \cos(\gamma_m z), \end{aligned} \quad (14)$$

where

$$\begin{aligned} A_{nm} &= \sum_{k=-\infty}^{\infty} a_{km} J_{k-n}(\alpha e), \\ B_{nm} &= \sum_{k=-\infty}^{\infty} b_{km} J_{k-n}(\alpha e), \\ C_{nm} &= \sum_{k=-\infty}^{\infty} c_{km} J_{k-n}(\beta e), \\ D_{nm} &= \sum_{k=-\infty}^{\infty} d_{km} J_{k-n}(\beta e), \\ E_{nm} &= \sum_{k=-\infty}^{\infty} e_{km} J_{k-n}(\beta e), \\ F_{nm} &= \sum_{k=-\infty}^{\infty} f_{km} J_{k-n}(\beta e) \end{aligned} \quad (15)$$

and one should note that the index “ $k$ ” has been interchanged with index “ $n$ ” for convenience. Direct substitution of field expansions (14) into the field equations (7), leads to

$$\begin{aligned} \sigma_{rr}(r_2, \theta_2, z, \omega) &= \sum_{m=-\infty}^{\infty} \sum_{n=-\infty}^{\infty} (A_{nm} S_{1nm}^{[1]} + B_{nm} S_{1nm}^{[2]} + C_{nm} S_{2nm}^{[1]} + D_{nm} S_{2nm}^{[2]} + E_{nm} S_{3nm}^{[1]} + F_{nm} S_{3nm}^{[2]}) \sin(\gamma_m z) e^{in\theta_2}, \\ \sigma_{r\theta}(r_2, \theta_2, z, \omega) &= \sum_{m=-\infty}^{\infty} \sum_{n=-\infty}^{\infty} (A_{nm} S_{4nm}^{[1]} + B_{nm} S_{4nm}^{[2]} + C_{nm} S_{5nm}^{[1]} + D_{nm} S_{5nm}^{[2]} + E_{nm} S_{6nm}^{[1]} + F_{nm} S_{6nm}^{[2]}) \sin(\gamma_m z) e^{in\theta_2}, \\ \sigma_{rz}(r_2, \theta_2, z, \omega) &= \sum_{m=-\infty}^{\infty} \sum_{n=-\infty}^{\infty} (A_{nm} S_{7nm}^{[1]} + B_{nm} S_{7nm}^{[2]} + C_{nm} S_{8nm}^{[1]} + D_{nm} S_{8nm}^{[2]} + E_{nm} S_{9nm}^{[1]} + F_{nm} S_{9nm}^{[2]}) \cos(\gamma_m z) e^{in\theta_2}. \end{aligned} \quad (16)$$

Next, imposing the outer surface condition (11c), while keeping in mind the orthogonality of transcendental functions, leads to the following complementary equations:

$$\begin{aligned} A_{nm} S_{1nm}^{[1]}(b, \omega) + B_{nm} S_{1nm}^{[2]}(b, \omega) + C_{nm} S_{2nm}^{[1]}(b, \omega) + D_{nm} S_{2nm}^{[2]}(b, \omega) + E_{nm} S_{3nm}^{[1]}(b, \omega) + F_{nm} S_{3nm}^{[2]}(b, \omega) &= 0, \\ A_{nm} S_{4nm}^{[1]}(b, \omega) + B_{nm} S_{4nm}^{[2]}(b, \omega) + C_{nm} S_{5nm}^{[1]}(b, \omega) + D_{nm} S_{5nm}^{[2]}(b, \omega) + E_{nm} S_{6nm}^{[1]}(b, \omega) + F_{nm} S_{6nm}^{[2]}(b, \omega) &= 0, \\ A_{nm} S_{7nm}^{[1]}(b, \omega) + B_{nm} S_{7nm}^{[2]}(b, \omega) + C_{nm} S_{8nm}^{[1]}(b, \omega) + D_{nm} S_{8nm}^{[2]}(b, \omega) + E_{nm} S_{9nm}^{[1]}(b, \omega) + F_{nm} S_{9nm}^{[2]}(b, \omega) &= 0, \end{aligned} \quad (17)$$

for  $n, m = \dots, -2, -1, 0, 1, 2, \dots$

Now, the simultaneous solutions of infinite-order systems (12) and (17) are required for complete dynamic characterization of the problem. These equations may advantageously be truncated into square-matrix form by setting

( $n = -N, \dots, -2, -1, 0, 1, 2, \dots, N$ ) in (12) and using ( $k = -N, \dots, -2, -1, 0, 1, 2, \dots, N$ ) in (15) in conjunction with (17), to obtain

$$\mathbf{S}_m \mathbf{c}_m = \mathbf{0} \quad (18)$$

where  $m = \dots, -2, -1, 0, 1, 2, \dots$ ,  $\mathbf{S}_m$  is a  $(6N + 1) \times (6N + 1)$  square matrix that contains extremely complicated frequency-dependent parameters which multiply the modal vector  $\mathbf{c}_m$ , and

$$\mathbf{c}_m = [a_{-Nm}, b_{-Nm}, c_{-Nm}, d_{-Nm}, e_{-Nm}, f_{-Nm}; a_{(-N+1)m}, b_{(-N+1)m}, c_{(-N+1)m}, d_{(-N+1)m}, e_{(-N+1)m}, f_{(-N+1)m}; \dots; a_{0m}, b_{0m}, c_{0m}, d_{0m}, e_{0m}, f_{0m}; \dots; a_{Nm}, b_{Nm}, c_{Nm}, d_{Nm}, e_{Nm}, f_{Nm}]^T \quad (19)$$

Finally, for nontrivial solutions of (18), the corresponding determinant,  $|\mathbf{S}_m|$ , must be set equal to zero, leading to the so-called frequency equation. The resonant frequencies are obtained by searching for the real roots of the frequency equation. Also, for the sake of completeness, the complete derivation of the 2D elasticity solution for the infinite eccentric cylinder is presented in Appendix B. This completes the necessary background required for exact analysis of the problem. Next, we consider some numerical examples.

### 3. Numerical results

In order to illustrate the nature and general behavior of solution, we consider a number of numerical examples in this section. A Mathematica code was constructed for numerical treatment of the system (18), i.e., to calculate the resonance frequencies and to determine the unknown Fourier coefficients (mode shapes) as a function of the dimensionless (cavity) eccentricity parameter  $\bar{e} = (b - a)/b$ . In particular, a simple and very efficient root finding technique based on the bisection approach [23] is employed to determine the roots of the characteristic equation ( $|\mathbf{S}_m| = 0$ ) by performing tedious frequency sweeping with extremely small frequency steps for detection of the value of the frequency parameter that causes the determinant to change sign. This procedure was repeated for all eccentricities using very small eccentricity steps ( $\Delta \bar{e} \approx 2\%$ ). This way, any remaining missing frequencies were identified and immediately included. Furthermore, after finding the roots of the characteristic equation by the above mentioned procedure, each root is substituted back into the coefficient matrix ( $\mathbf{S}_m$ ) and the corresponding eigenvector is obtained by using the powerful Mathematica built-in function NullSpace [ $\mathbf{S}_m$ ]. The computations were performed on a personal computer with a maximum truncation constant of  $k_{\max} = n_{\max} = N = 30$  to assure convergence in the high frequency range, and also in case of high core eccentricity. The convergence of numerical solutions were systematically checked in a simple trial and error manner, by increasing the truncation constant (i.e., including higher number of modes) while looking for steadiness or stability in the numerical value of the solutions.

Fig. 2a displays the variation of the truncation constant,  $N$ , with cavity eccentricity, required for proper convergence of the first dimensionless (fundamental) natural frequency,  $\Omega = \omega b/c_p$ , for selected infinite/finite cylinder geometries ( $a/b = 0.9$ ;  $L/b = 1$ ). It is clear that the issue of convergence is most critical for the highly eccentric cylinders. Fig. 2b displays the variation of the first several dimensionless natural frequencies,  $\Omega = \omega b/c_p$ , with the truncation constant,  $N$ , for selected infinite and finite cylinders of high radii ratio and eccentricity ( $\bar{e} = (b - a)/b = 90\%$ ;  $a/b = 0.9$ ;  $L/b = 1$ ). Here, it can be seen that the truncation constant required for adequate convergence of the computations increases with increasing the magnitude of natural frequency. Also, by performing numerous trial computer runs, it was concluded that the issue of convergence is most critical for the highly eccentric and high radii ratio cylinders. Moreover, when the cylindrical interfaces are in very close proximity to each other (i.e., as in the case of the highly eccentric cylinder with a large size cavity), it is found that increasingly more cylindrical Bessel functions should be included in the addition theorem (13) for proper convergence of the solutions. The latter observations may also be extended to the effect of cylinder length ratio,  $L/b$ , on the convergence. In particular, it is observed that in the case of shorter cylinders, increasingly more modes are required for proper convergence of solutions. This may be explained by the fact that as the cylinder length decreases, the magnitude of the fundamental frequency increases (see Fig. 3), causing a more stringent convergence requirement.

Fig. 3a shows the variation of the first several dimensionless natural frequencies ( $\Omega = \omega b/c_p$ ) with the eccentricity parameter ( $\bar{e} = (b - a)/b$ ) for selected inner–outer radius ratios ( $a/b = 0.2, 0.5, 0.9$ ). The associated circumferential mode numbers ( $n$ ) are also specified in each subplot. The modal spectrum of eccentric cylinder exhibits very unique characteristics. When the cylinder is perfectly axisymmetric (non-eccentric), the vibration modes can appear with repeated natural frequencies. As eccentricity is introduced, the asymmetry can cause the repeated vibration modes to split into modes with distinct natural frequencies. In particular, the eccentricity parameter inflicts characteristically different effects on natural frequencies depending on the radii ratio and mode number. Fig. 3b displays the corresponding 2D mode shapes for selected eccentricity parameters and mode numbers. It is clear from the first column of Fig. 3b that the deformation mode shapes for the concentric cylinder ( $\bar{e} = 0$ ) may essentially be divided into two general classes: the axisymmetric modes (i.e.,  $n = 0$ ) and the non-axisymmetric modes (e.g.,  $n = 1, 2, 3$ ). The latter modes may in turn be separated into symmetric and antisymmetric ones (denoted by “S” and “A” in Fig. 3b). Accordingly, we note from Fig. 3a that, regardless of radii ratio, the resonant frequency associated with the axisymmetric mode ( $n = 0$ ) remains single-valued in the entire range of eccentricity. In other words, there is a single non-repeated frequency associated with the axisymmetric mode. The frequency–eccentricity curve associated with the non-axisymmetric modes ( $n = 1, 2, 3$ ), on the other hand, bifurcate into

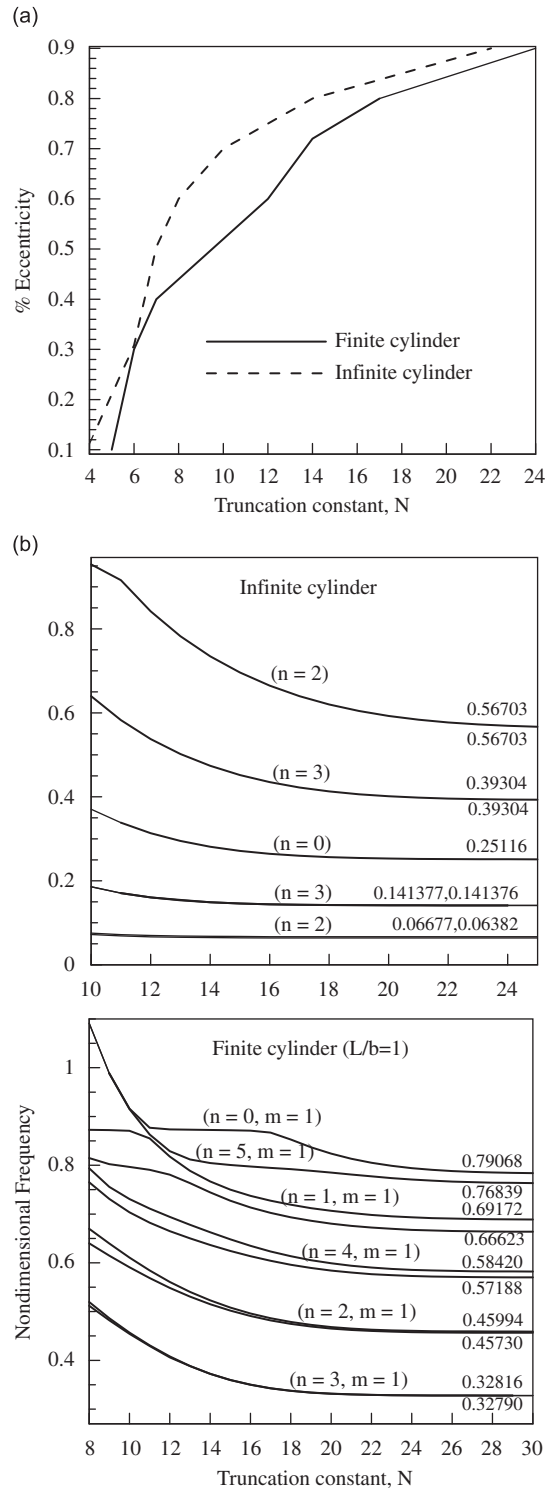


**Fig. 2.** (a) The truncation constant required for proper convergence of the first dimensionless (fundamental) natural frequency versus cavity eccentricity, for selected infinite/finite cylinder geometries ( $a/b = 0.9; L/b = 1$ ) and (b) the variation of the first several dimensionless natural frequencies ( $\Omega = \omega b/c_p$ ) with the truncation constant for selected cylinders of high radii ratio ( $a/b = 0.9$ ) and eccentricity ( $\bar{e} = (b - a)/b = 90\%$ ).

two branches as the eccentricity parameter increases. In particular, the initially encountered repeated double roots of the concentric cylinder ( $\bar{e} = 0$ ) exhibits a distinct decoupling of symmetric and anti-symmetric modes [13]. Also, the above noted separation (bifurcation) seems to be effectively delayed as the radii ratio ( $a/b$ ) increases.



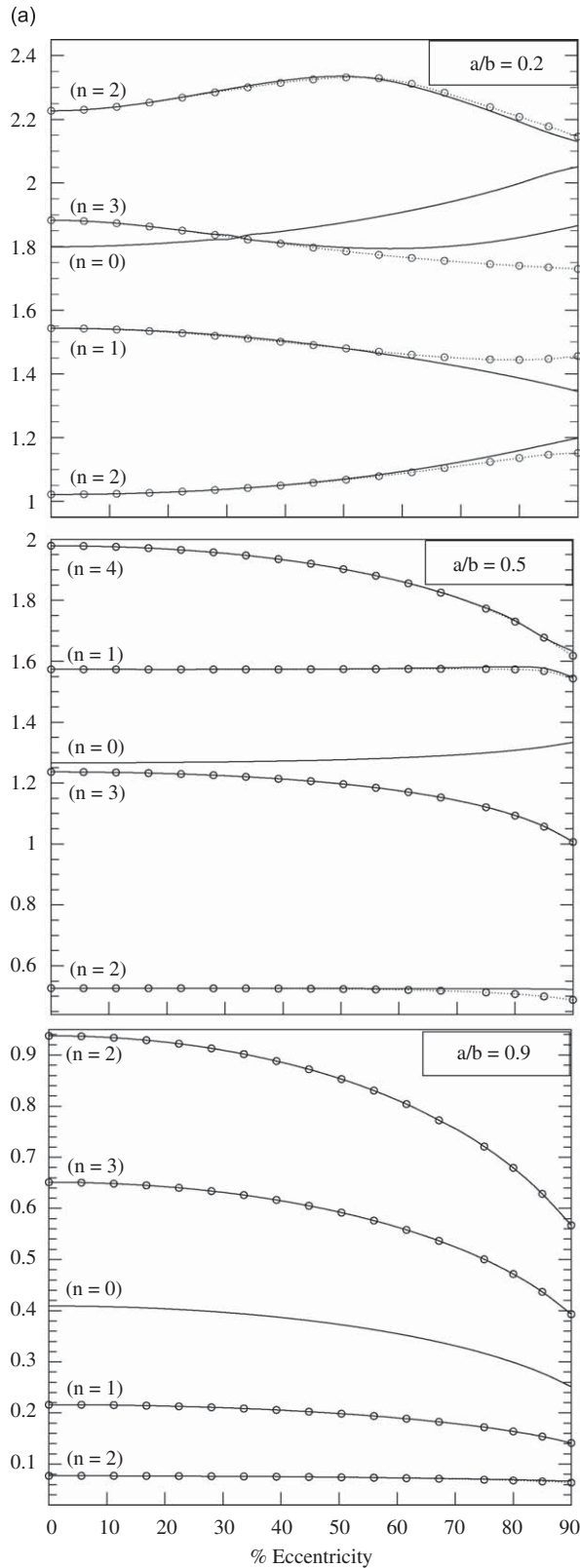


**Fig. 3.** (a) The variation of the first several dimensionless natural frequencies ( $\Omega = \omega b/c_p$ ) with the eccentricity parameter ( $\bar{e} = (b - a)/b$ ) for selected inner–outer radius ratios of the infinite cylinder (*dotted line*: branch 1; *solid line*: branch 2) and (b) the 2D mode shapes for selected eccentricities, mode numbers, and radii ratio ( $a/b = 0.2$ ), along with the FEM comparisons of the corresponding frequency parameters.

(b)

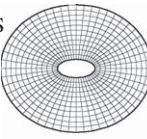
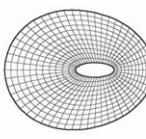
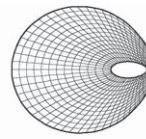
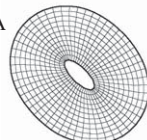
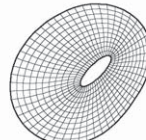
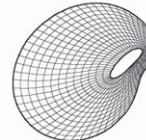
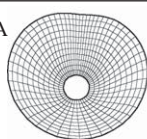
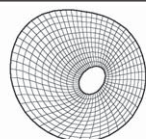
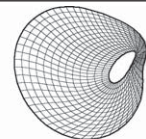
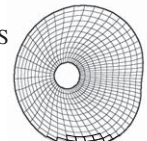
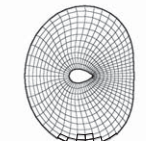
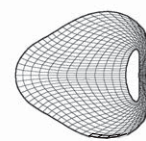
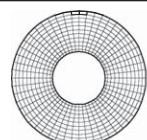
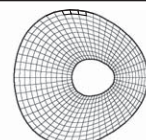
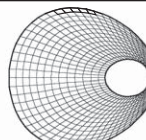
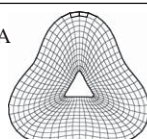
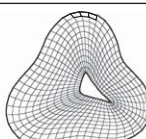
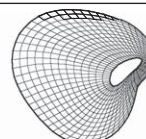
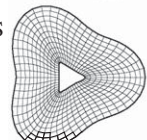
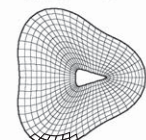
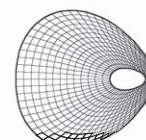
(n)	0% Eccentricity	28% Eccentricity	80% Eccentricity
(2)	 Analytical 1.02134 FEM 1.02134	 Analytical 1.03546 FEM 1.03547	 Analytical 1.13595 FEM 1.13602
	 Analytical 1.02134 FEM 1.02134	 Analytical 1.035691 FEM 1.035699	 Analytical 1.159671 FEM 1.159733
(1)	 Analytical 1.543659 FEM 1.543659	 Analytical 1.520129 FEM 1.520135	 Analytical 1.444586 FEM 1.444633
	 Analytical 1.543659 FEM 1.543659	 Analytical 1.523786 FEM 1.523793	 Analytical 1.387152 FEM 1.387184
(0)	 Analytical 1.799339 FEM 1.799341	 Analytical 1.822309 FEM 1.822311	 Analytical 1.998909 FEM 1.998918
(3)	 Analytical 1.882950 FEM 1.882950	 Analytical 1.836892 FEM 1.836922	 Analytical 1.739811 FEM 1.739929
	 Analytical 1.882950 FEM 1.882950	 Analytical 1.838785 FEM 1.838813	 Analytical 1.828739 FEM 1.828835

Fig. 3. (Continued)

Another interesting observation is the “crossover” of natural frequency curves corresponding to different mode shapes for  $a/b = 0.2$  in Fig. 3a (e.g., note the  $n = 0$  and 3 curves trading places at about  $\bar{e} = 30\%$ ). This implies that beyond the 30% eccentricity, the stiffness of structure in the  $n = 3$  vibration mode will decrease in comparison with that in the  $n = 0$  mode. Moreover, it appears that the largest overall shift in natural frequencies due to the increase in eccentricity occurs for high mode numbers at highest radii ratio (e.g.,  $n = 2, 3$  at  $a/b = 0.9$ ). Lastly, it should be noted that the circumferential modes with different wavenumbers are entirely decoupled when the cavity is concentric ( $\bar{e} = 0$ ). These modes get fully coupled as the cylinder becomes slightly eccentric (see Eq. (18)). As the eccentricity is further increased, progressively more of the coupled circumferential modes are included in the coefficient matrix  $S_m (6N + 1) \times (6N + 1)$  for proper convergence of the calculations (see Fig. 2a).

Fig. 4a shows the variation of the first several dimensionless natural frequencies with the eccentricity parameter for selected length-to-radius and inner-outer radius ratios ( $a/b = 0.2, 0.5, 0.9$ ;  $L/b = 1, 2, 5$ ). The associated circumferential/flexural mode numbers ( $n, m$ ) are also specified in each subplot. Fig. 4b displays the corresponding 3D mode shapes for selected eccentricity parameters and mode numbers. Comments very similar to above remarks can readily be made. The main distinctions are as follows. The bifurcation of resonant frequencies with increasing the eccentricity parameter for any given non-axisymmetric mode is effectively delayed as both the radii ratio ( $a/b$ ) and length-to-radius ratio ( $L/b$ ) are increased. This bifurcation seems to be most visible for the smallest length-to-radius ratio ( $L/b = 1$ ), where the largest separation is noted at the highest eccentricity ( $\bar{e} = 90\%$ ). Furthermore, in contrast with the 2D case (Fig. 3a), the frequency curve crossovers are no longer limited to small radii ratios, and there appears to be an increase in the number of crossover

points. This number considerably decreases, as the length to radius (radii) ratio is increased (decreased) to  $L/b = 5$  ( $a/b = 0.2$ ). Lastly, it appears that the largest overall shift in natural frequencies due to the increase in eccentricity occurs for highest radii ratio and lowest length ratio (i.e.,  $a/b = 0.9$  and  $L/b = 1$ ).

Finally, in order to check overall validity of the work, we first used our general Mathematica code to compute the frequency parameters ( $\Omega = \omega b/c_p$ ) associated with the selected two and 3D mode shapes presented in Figs. 3b and 4b. The results, which are tabulated next to the corresponding mode shapes in the latter figures, exhibit excellent agreements with the numerical calculations made by using the commercial finite element code ABAQUS [24]. It is noteworthy that in the latter validations, about 20,000 eight-noded 2D shell elements (CPS8R) of ABAQUS were used to model the infinite eccentric cylinder problem, while about 70,000 20-noded brick elements (C3D20R) were used to model the finite eccentric cylinder. As a further check, we set  $e = 0$  in our general code in order to calculate the normalized resonance frequencies,  $\bar{\Omega} = \omega(a+b)\sqrt{(1-\nu^2)\rho/E}/2$ , of a concentric hollow finite elastic cylinder ( $\nu = 0.3$ ;  $2(b-a)/(b+a) = 1.6$ ) for selected mode numbers,  $(n, m) = (0, 1), (1, 1), (2, 1)$ , and thickness parameters  $(b-a)/2L = 0.1, 0.2, 0.4, 0.6, 0.8, 1$ . The outcome, as presented in Table 1, exhibit excellent agreements with the natural frequencies given in Tables 6–8 of Ref. [5]. As a last check, we set  $a = 37.83$ ,  $b = 40.75$ ,  $L = 398.8$  (mm) in our general code in order to calculate the resonance frequencies ( $f = \omega/2\pi$  Hz) of a thin simply supported circular cylindrical steel shell of circumferentially varying wall thickness, for selected mode numbers and eccentricities ( $e = 0, 0.5$  mm). The result, as presented in Table 2, exhibit fair agreements with

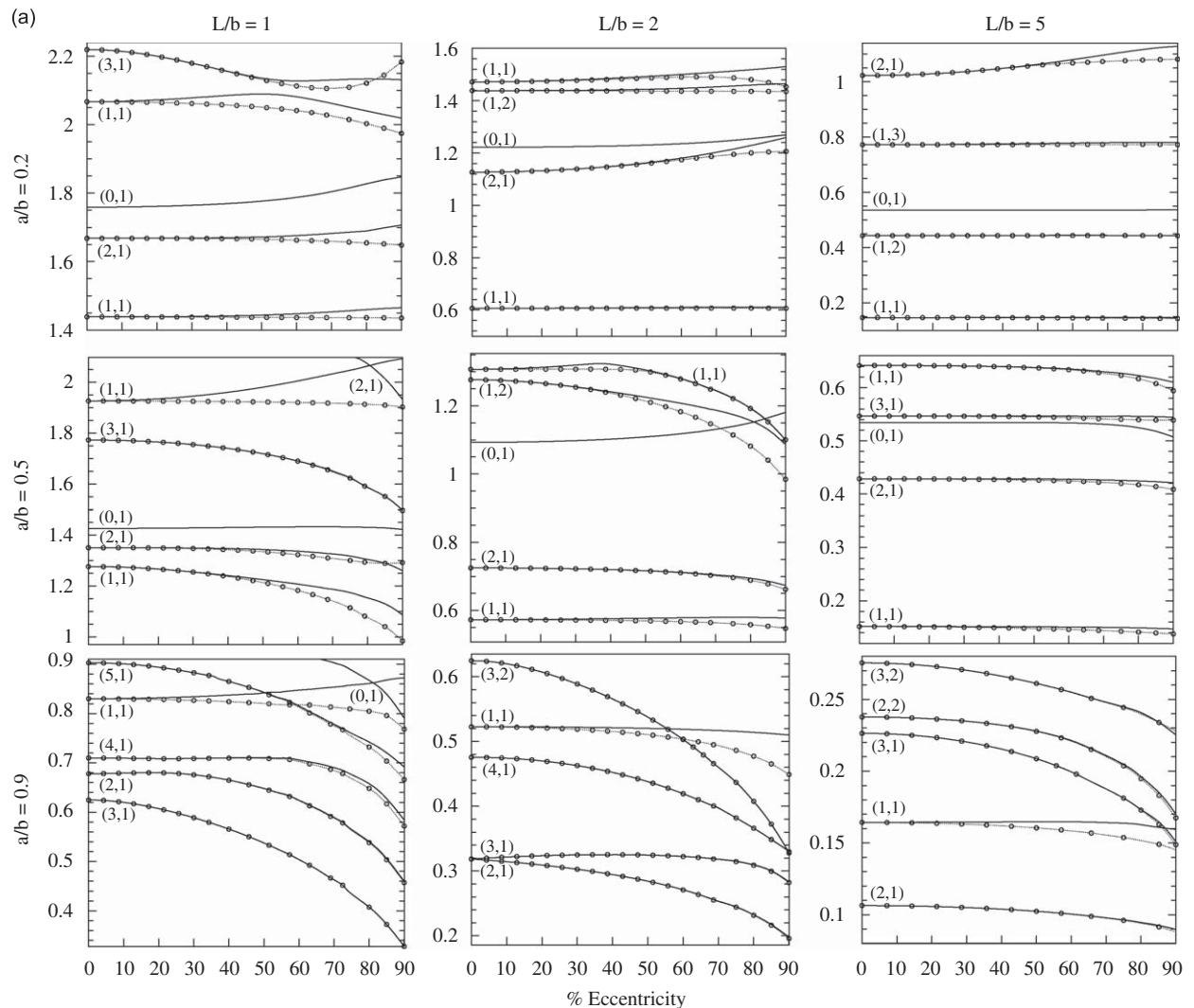


**Fig. 4.** (a) The variation of the first several dimensionless natural frequencies ( $\Omega = \omega b/c_p$ ) with the eccentricity parameter ( $\bar{e} = (b-a)/b$ ) for selected length-to-radius and inner-outer radius ratios of the finite cylinder (dotted line: branch 1; solid line: branch 2) and (b) the 3D mode shapes for selected eccentricities, mode numbers, radii and length ratios ( $a/b = 0.2, L/b = 1$ ), along with the FEM comparisons of the corresponding frequency parameters.

(b)

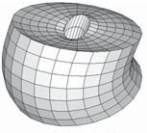
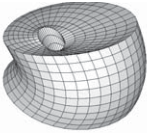
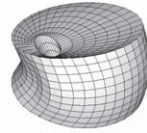
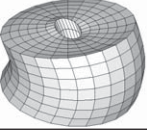
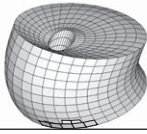
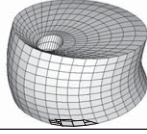
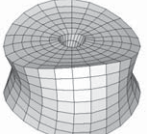
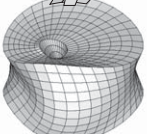
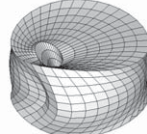
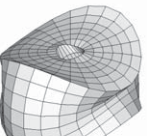
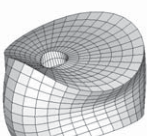
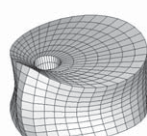
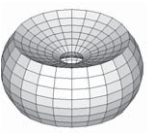
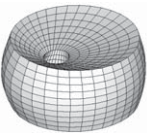
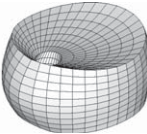
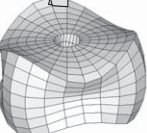
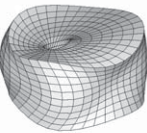
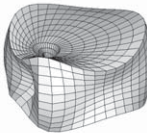
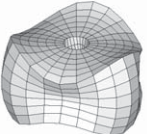
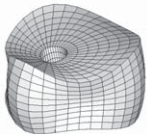
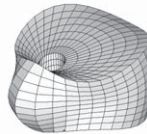
(n,m)	0%Eccentricity		50%Eccentricity		80%Eccentricity	
(1,1)		Analytical 1.438595 FEM 1.438666		Analytical 1.437045 FEM 1.437072		Analytical 1.436026 FEM 1.436063
		Analytical 1.438595 FEM 1.438666		Analytical 1.443543 FEM 1.443560		Analytical 1.459638 FEM 1.459649
(2,1)		Analytical 1.667873 FEM 1.667958		Analytical 1.665413 FEM 1.665434		Analytical 1.654584 FEM 1.654618
		Analytical 1.667873 FEM 1.667958		Analytical 1.671870 FEM 1.671911		Analytical 1.689486 FEM 1.689611
(0,1)		Analytical 1.759202 FEM 1.759188		Analytical 1.776556 FEM 1.776543		Analytical 1.827184 FEM 1.827152
(3,1)		Analytical 2.219171 FEM 2.219195		Analytical 2.131969 FEM 2.131954		Analytical 2.121183 FEM 2.121292
		Analytical 2.219171 FEM 2.219195		Analytical 2.135896 FEM 2.135869		Analytical 2.133574 FEM 2.133529

Fig. 4. (Continued)

Table 1

Comparison of frequency parameter calculations ( $\bar{\Omega} = \omega(a+b)\sqrt{(1-\nu^2)\rho/E/2}$ ) for the concentric hollow cylinder ( $e = 0$ ) with those in Ref. [5].

(n, m)		(b-a)/2L					
		0.1	0.2	0.4	0.6	0.8	1
(0, 1)	Ref. [5]	0.11659	0.23254	0.46476	0.69704	0.92935	1.16166
	present	0.11616	0.23232	0.46464	0.69697	0.92929	1.16161
(1, 1)	Ref. [5]	0.03150	0.11027	0.32509	0.55920	0.79446	1.02738
	present	0.03146	0.11025	0.32508	0.55918	0.79440	1.02724
(2, 1)	Ref. [5]	0.71819	0.71560	0.74697	0.84477	0.99411	1.17411
	present	0.71752	0.71495	0.74638	0.84425	0.99361	1.17358



**Table 2**

Comparison of the calculated resonance frequencies ( $f = \omega/2\pi$  Hz) of a thin simply supported circular cylindrical steel shell of circumferentially varying wall thickness, for selected mode numbers and eccentricities, with those in Refs. [13,17], along with the ABAQUS results.

$(m,n)$	$e = 0$ (mm)				$e = 0.5$ (mm)		
	Ref. [13]	Ref. [17]	ABAQUS	Present	Ref. [13]	Ref. [17]	Present
(1, 2)	1340	1330	1329	1330.7	1347	1335	1335.7
(1, 3)	3553	3529	3509	3515.0	3420	3442	3483.9
(1, 4)	6773	6746	6644	6657.8	6510	6463	6592.5
(2, 2)	2105	2050	2081	2083.5	2071	2043	2076.8
(2, 3)	3740	3698	3692	3699.1	3605	3565	3667.7
(2, 4)	6905	6846	6770	6784.9	6638	6567	6718.2
(3, 2)	3598	3517	3553	3555.5	3542	3469	3544.4

the natural frequency estimations given in Refs. [13,17], which were calculated by using Rayleigh–Ritz and Hybrid finite element methods, respectively. Also shown are the corresponding ABAQUS results, which again exhibit excellent agreements with our exact calculations.

#### 4. Conclusions

This paper presents an exact 3D elasticity series solution for free vibration analysis of a simply supported circular hollow cylinder of finite length with an eccentric inner circular cavity. A detailed study on the 2D free vibration characteristics of an infinite eccentric cylinder is also included. The first several resonant frequencies are calculated as a function of cavity eccentricity for selected geometric parameters. The most important observations are summarized as follows. The issue of convergence is found to be most critical for the upper modes of highly eccentric cylinders, especially when the radii ratio is large (large cavity), and/or length to radius ratio is small (short cylinder). The eccentricity parameter inflicts characteristically different effects on the natural frequencies depending on the mode type, and radii/length ratios. In particular, the calculated non-repeated eigenfrequency associated with the axisymmetric modes of the concentric cylinder is observed to remain single-valued through the entire eccentricity range. The repeated double roots (doublet frequencies) corresponding to the non-axisymmetric modes of the concentric cylinder exhibit distinct decoupling of symmetric and anti-symmetric modes. As the eccentricity is introduced, the doublet frequencies bifurcate into two distinct branches and the circumferential modes with different wavenumbers get fully coupled. As the eccentricity is increased, progressively more of the coupled circumferential modes should be included for proper convergence of the calculations. The bifurcation of resonance frequencies is most noticeable for the smallest length-to-radius ratio (shortest cylinder), where the largest separation is generally noted at the highest eccentricity. Also, the frequency splitting is effectively delayed as either the radii and/or length-to-radius ratios are increased. Another interesting observation is the appearance of “mode crossing” effect in the frequency–eccentricity plots. At the crossover point, two or more modes may share the same resonance frequency. Across this point, the vibrational stiffness (frequency ordering) of the involved modes are found to interchange value. The number of such crossovers is observed to considerably increase as the cylinder length (radii ratio) decreases (increases). Lastly, the largest overall shift in natural frequencies due to change in eccentricity is found to occur for the highest radii and lowest length ratios.

#### Appendix A

The expressions for  $V_{in}^{[k]}$  and  $S_{in}^{[k]}$  are given as

$$\begin{aligned}
 V_{1n}^{[i]}(r_j, \gamma, \omega) &= \alpha \ell_{n-1}^{[i]}(\alpha r_j) - \frac{n}{r_j} \ell_n^{[i]}(\alpha r_j), \\
 V_{2n}^{[i]}(r_j, \gamma, \omega) &= i \frac{n}{r} \ell_n^{[i]}(\beta r_j), \\
 V_{3n}^{[i]}(r_j, \gamma, \omega) &= -\gamma \beta \ell_{n-1}^{[i]}(\beta r_j) + \frac{n}{r_j} \ell_n^{[i]}(\beta r_j), \\
 V_{4n}^{[i]}(r_j, \gamma, \omega) &= i \frac{n}{r_j} \ell_n^{[i]}(\alpha r_j), \\
 V_{5n}^{[i]}(r_j, \gamma, \omega) &= -\beta \ell_{n-1}^{[i]}(\beta r_j) + \frac{n}{r_j} \ell_n^{[i]}(\beta r_j), \\
 V_{6n}^{[i]}(r_j, \gamma, \omega) &= -\gamma \frac{n}{r_j} \ell_n^{[i]}(\beta r_j), \\
 V_{7n}^{[i]}(r_j, \gamma, \omega) &= \gamma \ell_n^{[i]}(\alpha r_j), \\
 V_{8n}^{[i]}(r_j, \gamma, \omega) &= 0,
 \end{aligned}$$

$$V_{9n}^{[i]}(r_j, \gamma, \omega) = \beta^2 \ell_n^{[i]}(\beta r_j),$$

and

$$\begin{aligned} S_{1n}^{[i]}(r_j, \gamma, \omega) &= -2\mu \frac{\alpha}{r_j} \ell_{n-1}^{[i]}(\alpha r_j) + \left\{ 2\mu \frac{n(1+n)}{r_j^2} - [\lambda\gamma^2 + (\lambda + 2\mu)\alpha^2] \right\} \ell_n^{[i]}(\alpha r_j), \\ S_{2n}^{[i]}(r_j, \gamma, \omega) &= 2i\mu n \left[ \frac{\beta}{r_j} \ell_{n-1}^{[i]}(\beta r_j) - \frac{(1+n)}{r_j^2} \ell_n^{[i]}(\beta r_j) \right], \\ S_{3n}^{[i]}(r_j, \gamma, \omega) &= 2\mu\gamma \left\{ \frac{\beta}{r_j} \ell_{n-1}^{[i]}(\beta r_j) + \left[ -\frac{n(1+n)}{r_j^2} + \beta^2 \right] \ell_n^{[i]}(\beta r_j) \right\}, \\ S_{4n}^{[i]}(r_j, \gamma, \omega) &= 2i\mu n \left[ \frac{\alpha}{r_j} \ell_{n-1}^{[i]}(\alpha r_j) - \frac{(1+n)}{r_j^2} \ell_n^{[i]}(\alpha r_j) \right], \\ S_{5n}^{[i]}(r_j, \gamma, \omega) &= 2\mu \frac{\beta}{r_j} \ell_{n-1}^{[i]}(\beta r_j) + \mu \left[ -2 \frac{n(1+n)}{r_j^2} + \beta^2 \right] \ell_n^{[i]}(\beta r_j), \\ S_{6n}^{[i]}(r_j, \gamma, \omega) &= 2in\gamma\mu \left[ -\frac{\beta}{r_j} \ell_{n-1}^{[i]}(\beta r_j) + \frac{(1+n)}{r_j^2} \ell_n^{[i]}(\beta r_j) \right], \\ S_{7n}^{[i]}(r_j, \gamma, \omega) &= 2\gamma\mu \left[ \alpha \ell_{n-1}^{[i]}(\alpha r_j) - \frac{n}{r_j} \ell_n^{[i]}(\alpha r_j) \right], \\ S_{8n}^{[i]}(r_j, \gamma, \omega) &= i\mu\gamma \frac{n}{r_j} \ell_n^{[i]}(\beta r_j), \\ S_{9n}^{[i]}(r_j, \gamma, \omega) &= \mu(\beta^2 - \gamma^2) \left[ \beta \ell_{n-1}^{[i]}(\beta r_j) - \frac{n}{r_j} \ell_n^{[i]}(\beta r_j) \right], \\ S_{10n}^{[i]}(r_j, \gamma, \omega) &= -[\lambda\alpha^2 + (\lambda + 2\mu)\gamma^2] \ell_n^{[i]}(\alpha r_j), \\ S_{11n}^{[i]}(r_j, \gamma, \omega) &= 0, \\ S_{12n}^{[i]}(r_j, \gamma, \omega) &= -2\gamma\mu\beta^2 \ell_n^{[i]}(\beta r_j), \end{aligned}$$

where  $i, j = 1, 2$ , and

$$\ell_n^{[i]} = \begin{cases} J_n & (i = 1) \\ Y_n & (i = 2). \end{cases}$$

## Appendix B

The 2D scalar field potentials with respect to the  $(r_1, \theta_1)$  and  $(r_2, \theta_2)$  polar coordinate systems are respectively written as

$$\begin{aligned} \varphi(r_1, \theta_1, \omega) &= \sum_{n=-\infty}^{\infty} [a_n J_n(\alpha r_1) + b_n Y_n(\alpha r_1)] e^{in\theta_1}, \\ \psi(r_1, \theta_1, \omega) &= \sum_{n=-\infty}^{\infty} [c_n J_n(\beta r_1) + d_n Y_n(\beta r_1)] e^{in\theta_1} \end{aligned} \quad (\text{B.1})$$

and

$$\begin{aligned} \varphi(r_2, \theta_2, \omega) &= \sum_{n=-\infty}^{\infty} [A_n J_n(\alpha r_2) + B_n Y_n(\alpha r_2)] e^{in\theta_2}, \\ \psi(r_2, \theta_2, \omega) &= \sum_{n=-\infty}^{\infty} [C_n J_n(\beta r_2) + D_n Y_n(\beta r_2)] e^{in\theta_2}, \end{aligned} \quad (\text{B.2})$$

where  $\alpha^2 = \omega^2/c_p^2$  and  $\beta^2 = \omega^2/c_s^2$ , and

$$\begin{aligned} A_n &= \sum_{k=-\infty}^{\infty} a_k J_{k-n}(\alpha e), \\ B_n &= \sum_{k=-\infty}^{\infty} b_k J_{k-n}(\alpha e), \end{aligned}$$

$$C_n = \sum_{k=-\infty}^{\infty} c_k J_{k-n}(\beta e),$$

$$D_n = \sum_{k=-\infty}^{\infty} d_k J_{k-n}(\beta e). \tag{B.3}$$

Also, one should note that the index “k” has been interchanged with index “n” in (B.2) and (B.3) for convenience. The relevant stress components with respect to the  $(r_1, \theta_1)$  and  $(r_2, \theta_2)$  coordinate systems are, respectively, written as

$$\sigma_{rr}(r_1, \theta_1, \omega) = \sum_{n=-\infty}^{\infty} (a_n T_{1n}^{[1]} + b_n T_{1n}^{[2]} + c_n T_{2n}^{[1]} + d_n T_{2n}^{[2]}) e^{in\theta_1},$$

$$\sigma_{r\theta}(r_1, \theta_1, \omega) = \sum_{n=-\infty}^{\infty} (a_n T_{3n}^{[1]} + b_n T_{3n}^{[2]} + c_n T_{4n}^{[1]} + d_n T_{4n}^{[2]}) e^{in\theta_1} \tag{B.4}$$

and

$$\sigma_{rr}(r_2, \theta_2, \omega) = \sum_{n=-\infty}^{\infty} (A_n T_{1n}^{[1]} + B_n T_{1n}^{[2]} + C_n T_{2n}^{[1]} + D_n T_{2n}^{[2]}) e^{in\theta_2},$$

$$\sigma_{r\theta}(r_2, \theta_2, \omega) = \sum_{n=-\infty}^{\infty} (A_n T_{3n}^{[1]} + B_n T_{3n}^{[2]} + C_n T_{4n}^{[1]} + D_n T_{4n}^{[2]}) e^{in\theta_2}, \tag{B.5}$$

where

$$T_{1n}^{[i]}(r_j, \omega) = -2\mu \frac{\alpha}{r_j} \ell_{n-1}^{[i]}(\alpha r_j) + \left[ 2\mu \frac{n(1+n)}{r_j^2} - (\lambda + 2\mu)\alpha^2 \right] \ell_n^{[i]}(\alpha r_j),$$

$$T_{2n}^{[i]}(r_j, \omega) = 2i\mu n \left[ \frac{\beta}{r_j} \ell_{n-1}^{[i]}(\beta r_j) - \frac{(1+n)}{r_j^2} \ell_n^{[i]}(\beta r_j) \right],$$

$$T_{3n}^{[i]}(r_j, \omega) = 2i\mu n \left[ \frac{\alpha}{r_j} \ell_{n-1}^{[i]}(\alpha r_j) - \frac{(1+n)}{r_j^2} \ell_n^{[i]}(\alpha r_j) \right],$$

$$T_{4n}^{[i]}(r_j, \omega) = 2\mu \frac{\beta}{r_j} \ell_{n-1}^{[i]}(\beta r_j) + \mu \left[ -2 \frac{n(1+n)}{r_j^2} + \beta^2 \right] \ell_n^{[i]}(\beta r_j), \tag{B.6}$$

where  $i, j = 1, 2$ , and

$$\ell_n^{[i]} = \begin{cases} J_n & (i = 1) \\ Y_n & (i = 2) \end{cases}.$$

The pertinent boundary conditions are

$$\sigma_{rr}(r_1 = a, \theta_1, \omega) = \sigma_{r\theta}(r_1 = a, \theta_1, \omega) = 0, \tag{B.7a}$$

$$\sigma_{rr}(r_2 = b, \theta_2, \omega) = \sigma_{r\theta}(r_2 = b, \theta_2, \omega) = 0. \tag{B.7b}$$

Substitution of (B.4) through (B.5) into the boundary conditions (B.7a,b) leads to

$$a_n T_{1n}^{[1]}(a, \omega) + b_n T_{1n}^{[2]}(a, \omega) + c_n T_{2n}^{[1]}(a, \omega) + d_n T_{2n}^{[2]}(a, \omega) = 0,$$

$$a_n T_{3n}^{[1]}(a, \omega) + b_n T_{3n}^{[2]}(a, \omega) + c_n T_{4n}^{[1]}(a, \omega) + d_n T_{4n}^{[2]}(a, \omega) = 0, \tag{B.8a}$$

and

$$A_n T_{1n}^{[1]}(b, \omega) + B_n T_{1n}^{[2]}(b, \omega) + C_n T_{2n}^{[1]}(b, \omega) + D_n T_{2n}^{[2]}(b, \omega) = 0,$$

$$A_n T_{3n}^{[1]}(b, \omega) + B_n T_{3n}^{[2]}(b, \omega) + C_n T_{4n}^{[1]}(b, \omega) + D_n T_{4n}^{[2]}(b, \omega) = 0 \tag{B.8b}$$

for  $n = \dots, -2, -1, 0, 1, 2, \dots$ . These equations may advantageously be truncated into square-matrix form by setting  $(n = -N, \dots, -2, -1, 0, 1, 2, \dots, N)$  in (B.8a) and using  $(k = -N, \dots, -2, -1, 0, 1, 2, \dots, N)$  in (B.3) in conjunction with (B.8b),

to obtain

$$\mathbf{T}\mathbf{d} = \mathbf{0}, \quad (\text{B.9})$$

where  $\mathbf{T}$  is a  $(4N + 1) \times (4N + 1)$  square matrix that contains extremely complicated frequency-dependent parameters which multiply the modal vector  $\mathbf{d}$ , and

$$\mathbf{d} = [a_{-N}, b_{-N}, c_{-N}, d_{-N}; a_{-N+1}, b_{-N+1}, c_{-N+1}, d_{-N+1}; \dots; a_0, b_0, c_0, d_0; \dots; a_N, b_N, c_N, d_N]^T.$$

## References

- [1] A.W. Leissa, *Vibration of Shells*, (NASA SP-288), US Government Printing Office, 1973.
- [2] K.P. Soldatos, Review of three dimensional dynamic analyses of circular cylinders and cylindrical shells, *Applied Mechanics Reviews* 47 (1994) 501–516.
- [3] L. Pochhammer, On the propagation velocities of small oscillations in an unlimited isotropic circular cylinder, *Zeitschrift für Reine und Angewandte Mathematik* 81 (1876) 324–336.
- [4] J.R. Hutchinson, S.A. E1-Azhari, Vibrations of free hollow circular cylinder, *Journal of Applied Mechanics* 53 (1986) 641–647.
- [5] C.T. Loy, K.Y. Lam, Vibration of thick cylindrical shells on the basis of three dimensional theory of elasticity, *Journal of Sound and Vibration* 226 (1999) 719–737.
- [6] M.R. Mofakhami, H.H. Toudeshky, Sh.H. Hashemi, Finite cylinder vibrations with different end boundary conditions, *Journal of Sound and Vibration* 297 (2006) 293–314.
- [7] L. Cheng, Y.Y. Li, L.H. Yam, Vibration analysis of annular-like plates, *Journal of Sound and Vibration* 262 (2003) 1153–1170.
- [8] H.B. Khurasia, S. Rewtant, Vibration analysis of circular plates with hole, *Journal of Applied Mechanics* 45 (1978) 215–217.
- [9] P.A.A. Laura, C.P. Filipich, R.E. Rossi, J.A. Reyes, Vibrations of rings of variable cross section, *Applied Acoustics* 25 (1988) 225–234.
- [10] R.S. Hwang, C.H.J. Fox, S. McWilliam, The in-plane vibration of thin rings with in-plane profile variations—part I: general background and theoretical formulation, *Journal of Sound and Vibration* 220 (1999) 497–516.
- [11] H. Zhong, T. Yu, Flexural vibration analysis of an eccentric annular Mindlin plate, *Archive of Applied Mechanics* 77 (2007) 185–195.
- [12] V.T. Golovchan, Plane vibration of an eccentric cylinder, *Soviet Applied Mechanics* 5 (1972) 543–546.
- [13] R.F. Tonin, D.A. Bies, Free vibration of a circular cylinder with variable thickness, *Journal of Sound and Vibration* 62 (1979) 165–180.
- [14] K. Suzuki, A.W. Leissa, Exact solutions for the free vibrations of open cylindrical shells with circumferentially varying curvature and thickness, *Journal of Sound and Vibration* 107 (1986) 1–15.
- [15] K. Suzuki, A.W. Leissa, Analysis of free vibrations of noncircular thick cylindrical shells having circumferentially varying thickness, *International Journal of Solids and Structures* 26 (1990) 255–270.
- [16] V. Kumar, A.V. Singh, Vibration analysis of non-circular cylindrical shells using Bezier function, *Journal of Sound and Vibration* 161 (1993) 333–354.
- [17] M.H. Toorani, A.A. Lakis, Free vibrations of non-uniform composite cylindrical shells, *Nuclear Engineering and Design* 236 (2006) 1748–1758.
- [18] V. Wowk, *Machinery Vibration*, McGraw-Hill, New York, 2000.
- [19] H.F. Tiersten, D.V. Shick, Resonant wave propagation in gun tubes with eccentric bores, *Wave Motion* 21 (1995) 75–84.
- [20] P. Bisegna, G. Caruso, Frequency split and vibration localization in imperfect rings, *Journal of Sound and Vibration* 306 (2007) 691–711.
- [21] Y.H. Pao, C.C. Mow, *Diffraction of Elastic Waves and Dynamics Stress Concentration*, Crane Russak, New York, 1973.
- [22] Ye.A. Ivanov, *Diffraction of Electromagnetic Waves on Two Bodies*, Nauka i Tekhnika, 1968.
- [23] C.F. Gerald, P.O. Wheatley, *Applied Numerical Analysis*, Addison-Wesley, New York, 1994.
- [24] ABAQUS, Analysis User's Manual, Version 6.6, on-line documentation.